Nanoscale

COMMUNICATION

View Article Online
View Journal

Cite this: DOI: 10.1039/c5nr03759j

Received 8th June 2015,
Accepted 23rd June 2015

DOI: 10.1039/c5nr03759j

www.rsc.org/nanoscale

An ordered mesoporous Ag superstructure synthesized *via* a template strategy for surface-enhanced Raman spectroscopy†

Cuifeng Tian,[a,b] Jiang Li,[a] Chunsheng Ma,[a] Ping Wang,[b] Xiaohong Sun*[c] and Jixiang Fang*[a]

Surface-enhanced Raman scattering (SERS) substrates with high density and uniformity of nanogaps are proven to enhance the reproducibility and sensitivity of the Raman signal. Up to now, the syntheses of a highly ordered gold or silver superstructure with a controllable nanoparticle size and a well-defined particle gap have been quite limited. Here, we reported an ordered mesoporous silver superstructure replicated by using ordered mesoporous KIT-6 and SAB-15 as templates. By means of a nanocasting process, the ordered mesoporous Ag superstructure was successfully synthesized, which shows uniform distribution of the nanowire diameter (10 nm) and nanogap size (~2 nm), thus exhibiting a high Raman enhancement of ~10^9. The finite difference time-domain (FDTD) results indicate that the ordered mesoporous Ag superstructure has a uniform distribution of hot spots. Therefore, the mesoporous silica template strategy presented here could lead to a new class of high quality SERS substrates providing extraordinary potential for diverse applications.

Surface-enhanced Raman spectroscopy (SERS) is characterized by a rather large amplification of the weak spontaneous Raman signal. The origin of this enhancement is shown to rely on the surface plasmon resonance (SPR) between the laser and the metal nanostructure.[1,2] It is known that the surface plasmonic couplings usually occur at SERS-active sites, including several nanometer gap junctions (defined as 'hot spots') or tips around which a giant electromagnetic enhancement is induced.[3–5] However, the random distribution of hot spots results in a wide distribution of EF values and the appearance of irreproducible SERS signals.[6] In addition, the relatively low density of SERS-active sites obtained *via* a lithographic route makes the SERS signal poorly uniform, particularly at ultralow molecule concentrations, because, in this case, quite a few dye molecules might not land inside hot spots although they could be precisely prefabricated.[7] Therefore, the center problem now is the good definition of hot spots, including how to reproducibly synthesize sub-5 nm nanogaps between nanoparticles, how to increase the density of the hot spots and how to regulate the uniformity of the nanogap distance within the SERS substrate.

At present, some outstanding approaches are available for controlling the nanogap size and density,[8–15] such as the self-assembly method,[8,9] lithographic techniques,[10] the template strategy including AAO,[11] and the use of polymer templates[12] and 3D SiO_2 sphere templates.[13] Although these substrates have made a great improvement in the control of the gap size, there are fewer that are capable of meeting the requirements of a SERS-active substrate, for instance small nanogaps and high hot spot density. Recently, Fang's group has successfully synthesized highly ordered mesoporous silver supercrystals (OMASC-28) by using an ordered porous template with a large pore size up to 28 nm, which exhibited high SERS sensitivity.[15] Wang *et al.* have also obtained ordered polyhedral mesoporous Pt nanoparticles using the mesoporous template of KIT-6.[14] In fact, the obtained nanostructures can be well tailored to enhance the local field effect through selecting various templates. For example, the hot spot density can be further increased by means of a template with small pore sizes, *i.e.* less than ~10 nm. Moreover, using various templates, diverse mesostructures with controlled gap sizes and high hot spot density may be achieved (Fig. 1a).

Herein we used two kinds of ordered mesoporous templates, *e.g.* the mesoporous silica KIT-6 and SBA-15 structures to prepare the highly ordered mesoporous Ag superstructure (OMAS) through the dip-calcination method (described in the Experimental section). As a result, two typical mesostructures of the OMAS were obtained, including interconnected mesh structures and nanowire bundles as shown in Fig. 1a.

[a]*School of Science, Key Laboratory of the Ministry of Education and International Center for Dielectric Research, Xi'an Jiaotong University, Shann xi, 710049, China. E-mail: jxfang@mail.xjtu.edu.cn, sunxh@tju.edu.cn*

[b]*School of Physics and Electronic Science, Shanxi Datong University, Shanxi 037009, P. R. China*

[c]*School of Materials Science and Engineering, TianJin University, Tianjin, 300072, China*

† Electronic supplementary information (ESI) available: TEM images of the KIT-6 template, SEM images of OMAS-10, details of FDTD simulation, optical parameters, and the estimation of the SERS enhancement factor. See DOI: 10.1039/c5nr03759j

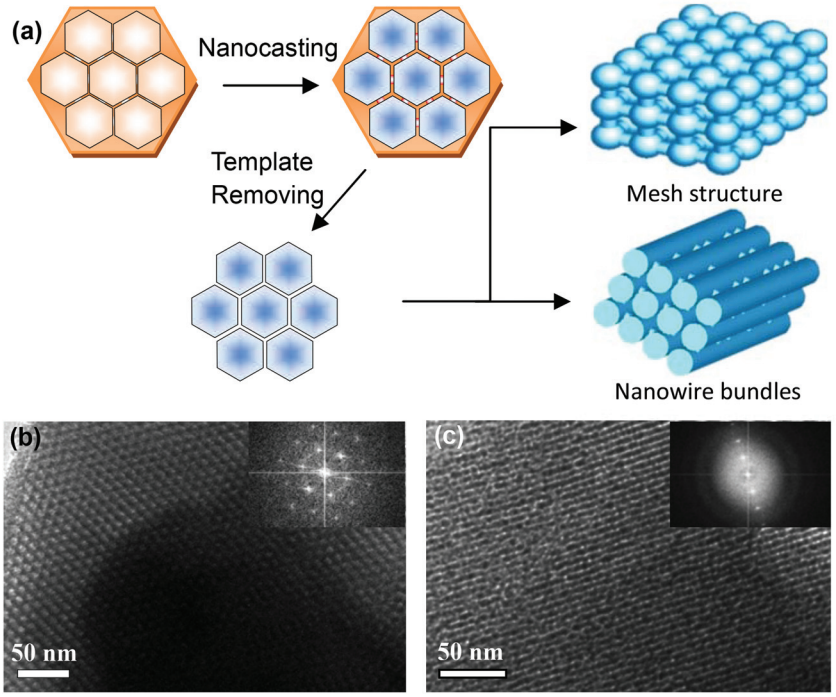

Fig. 1 (a) Schematic diagram of the synthesis procedure for ordered silver superstructures by means of a nanocasting process using KIT-6 and SBA-15 templates. The low-magnification TEM image of ordered mesoporous silica templates: (b) KIT-6; (c) SBA-15; insets of (b) and (c) show the corresponding FFT diffractograms.

The nanoparticle diameter and gap size of the Ag superstructure can be well controlled by the KIT-6 and SBA-15 templates (Fig. 1a). Owing to the uniform and high density of nanogaps between nanoparticle building blocks, the OMAS can be promising to employ as high-quality SERS substrates. The plasmon enhancement performance was evaluated *via* Raman spectroscopy and the electromagnetic field calculation using the finite difference time domain (FDTD) method. We found that the OMAS with an appropriate nanowire diameter, *i.e.* 10 nm, and a gap size of ~2 nm displayed a highly effective SERS activity with high signal amplification reaching ~10^9.

Results and discussion

In this work, we chose ordered mesoporous silica KIT-6 and SBA-15 structures as templates to prepare the ordered mesoporous Ag superstructure (here, the diameter of nanoparticles is about 10 nm, so denoted as OMAS-10). The KIT-6 template was synthesized according to the procedure in ref. 16. The transmission electron microscopy (TEM) image of the ordered mesoporous silica template KIT-6 indicates that the template has a highly ordered structure with preferable arrangement along the [311] direction (Fig. 1b) and the [531] direction (Fig. S1a†) as described in a previous report,[16] and displays cubic *Ia3d* symmetry. The pore size (about 8–10 nm) was estimated by the TEM image (Fig. 1b) and the small-angle X-ray scattering (SAXS) curve (Fig. S1b†). In Fig. 1c another ordered mesoporous template, *i.e.* SBA-15, by which nanowire morphology normally can be fabricated is shown.[17]

The morphologies and structures of the obtained OMAS-10 by using the calcination method (as described in the Experimental section) after the removal of the hard template of SBA-15 and KIT-6 are shown in Fig. 2 and 3. From the lower magnification SEM image of OMAS-10 for nanowire bundles (Fig. 2a), we can see that the size of nanowire bundles is about several micrometers and there are some discrete nanowires covered on the bundles. In Fig. 2b, it can be seen that the nanowires paralleled to each other and the diameter is about 9–10 nm, which is consistent with the pore size of the parent template. By means of the same processes of nanowire bundles, the mesh morphology of OMAS-10 can also be obtained through calcination (Fig. 2c and d). Similar morphologies show that the growth of silver nanoparticles was restricted within the parent template. Furthermore, the comparison of the structure for the KIT-6 template and the OMAS-10 may further confirm this statement. In Fig. S1† and in ref. 16, the templates have different pore connecting ways which determine the morphologies of the OMAS-10 (shown in Fig. S2†). In the inset of Fig. 2d, we can see one of the networks, which replicated the {111} surface of the KIT-6 template.

The structural features of OMAS-10 are further elucidated from the TEM images as shown in Fig. 3. From Fig. 3a and b, the individual nanowires distribute parallel to each other. The diameter of nanowires is about 10 nm and the gap between

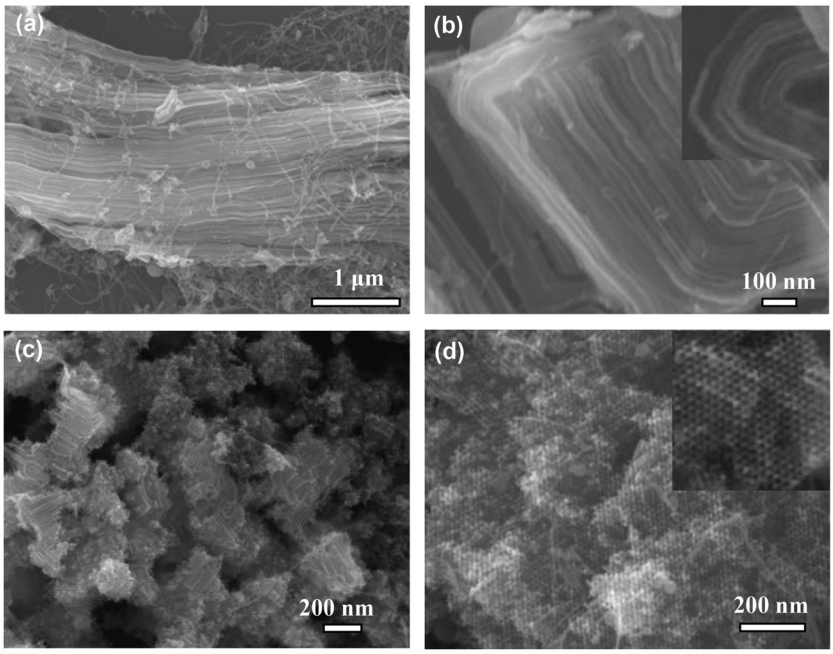

Fig. 2 Low and high magnification SEM images of ordered mesoporous silver structures: (a) and (b) nanowire bundles obtained from the SBA-15 template; (c) and (d) mesh structures obtained from the KIT-6 template.

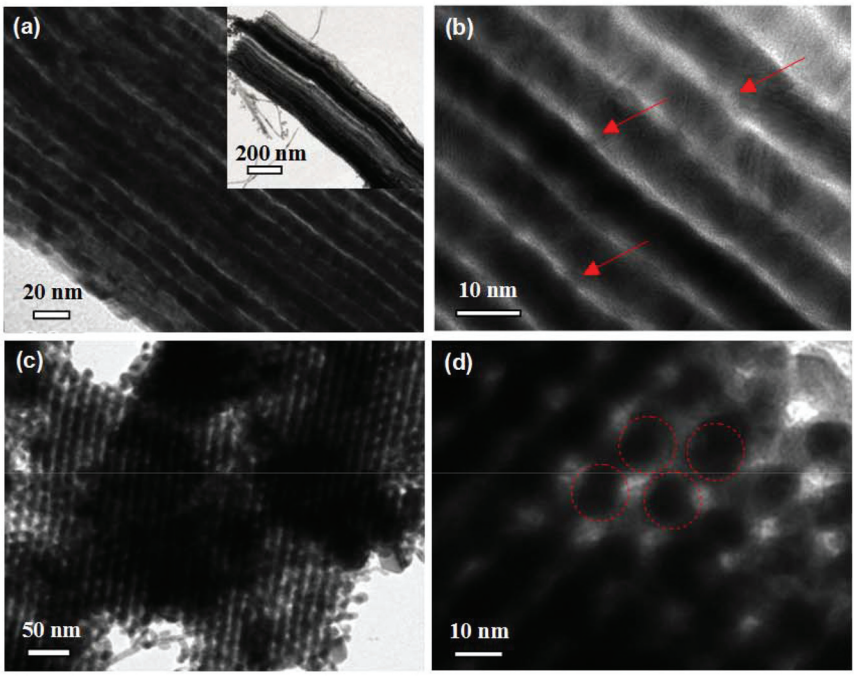

Fig. 3 TEM images of the as-made highly mesoporous silver structure (OMAS-10) after removing the template: (a) and (b) nanowire bundles, (c) and (d) mesh structures.

nanowires is around 2–3 nm. It is noted that some connecting nanoparticles can be observed between nanowires, which contribute to the structural stability of nanowire bundles even after the removal of the silica template. For the mesh morphology, the diameter of the silver sphere is about 10 nm (as shown with the dotted circles of Fig. 3d). The nanoparticles are connected by small necks with a distance between nanoparticle building blocks of around 2–5 nm (Fig. 3d). The selec-

tive area electron diffraction (SAED) of the OMAS-10 is shown in Fig. S3a,† which confirms its polycrystalline nature. As one can see from Fig. S3b,† the spacing of lattice planes is 0.23 nm for a single silver sphere, which is consistent with the space of the (111) crystal plane of silver.[18] According to our previous processes, the silica template may be removed completely after washing with a NaOH solution three times[15] and this can be confirmed by energy dispersive X-ray spectrometry (EDS, in Fig. S4†), displaying no obvious oxygen element existing in the OMAS-10 specimens.

To gain deep insights into the properties of local surface plasmon resonance (LSPR) for the two mesostructures of OMAS-10, the finite difference time-domain (FDTD) calculation was carried out to understand the interaction between the electromagnetic field and the OMAS-10 (the models are shown in Fig. S5†). From the comparison of electrical field intensity, one can see that the OMAS-10 with a nanowire bundle structure displays a relatively higher enhancement capability than that of the mesh structure at the excitation light wavelength of 514 nm and 633 nm (Fig. 4a and c). Considering the uncertainty of the size of connecting rods, we studied the dependence of the connecting rod widths (w) on the electrical field amplification at the same silver sphere diameters (D = 10 nm) and gap size (g = 2 nm). The results showed that the field magnitude for the rod widths from 4–6 nm exhibits a comparable scale (Fig. 4a and c), revealing that the width of the connecting rod has little impact on the field enhancement of the Ag superstructure when the diameter of silver and the gap size are given. Furthermore, one can see that the OMAS-10 for both structures demonstrates the highest field enhancement with $|E|/|E_0| \sim 40$ at an excitation wavelength of 785 nm, which corresponds to a SERS enhancement (proportional to $\sim|E|^4$) of $\sim 10^6$. As for the calculated field enhancement factor, it is lower than the one obtained from the experiment (see below), which could be attributed to the chemical contribution and the difference between the model and actual arrangements of OMAS-10.[19,20] Fig. 4b and d show the calculated electromagnetic field distribution of the OMAS-10 at 514 nm excitation wavelength. Obviously, the maxima field enhancements are uniformly located in the gaps between two Ag spheres or two Ag nanowires. In addition, owing to the small nanoparticle building blocks, *i.e.* ~10 nm for two structures, the FDTD results indicate that both the two models contribute to an ultrahigh hot spot density which can also be of great benefit to the reproducibility for the SERS signal. Therefore, the OMAS-10 structure reported in this work could serve as an efficient SERS substrate to achieve a high sensitivity and repeatability of the detected signal.

The SERS performance for two typical structures of the OMAS-10 was evaluated and is shown in Fig. 5. We examined the widely used dye molecules, crystal violet (CV), for SERS studies. Precise determination of the structure of OMAS-10 as

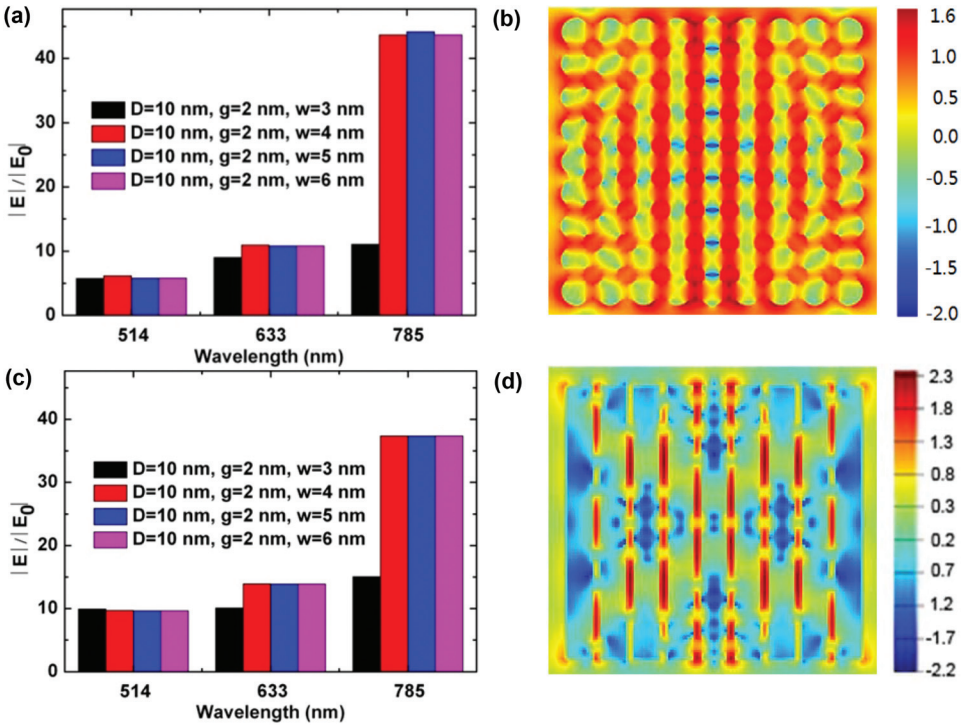

Fig. 4 The histograms of field enhancements of two kinds of OMAS-10 as the functions of widths of the connecting rod varied from 3 to 6 nm for three excitation wavelengths: (a) mesh structure. (c) Nanowire bundles. (b) and (d) are the calculated E-field distributions and their E-field intensity of OMAS-10, D = 10 nm, g = 2 nm, w = 5 nm for mesh and nanowire structures, respectively. The scale bars of the electromagnetic field intensity $|E|^2$ have been plotted on the log-scale.

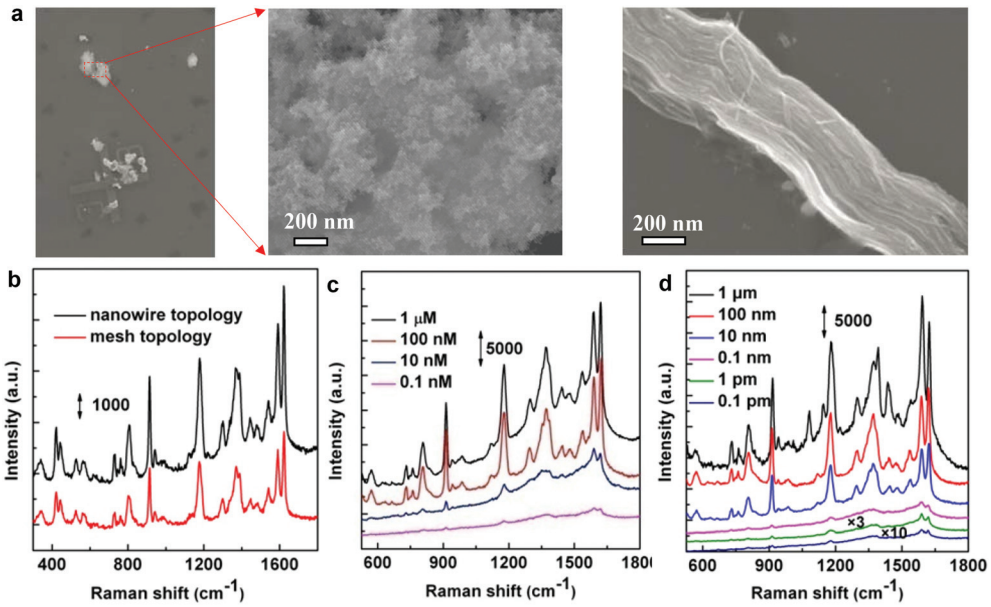

Fig. 5 SEM image of the OMAS-10 on the marked silicon wafer: (a) mesh structure and nanowire bundles. SERS spectra of CV adsorbed on the OMAS-10 substrates, (b) the spectra of 10^{-7} M CV measured with a confocal Raman microscope (LabRAM HR800): a 514 nm excitation laser, 2 s acquisition time, 0.022 mw laser power and 100× objective lens. (c) and (d) SERS spectra of the OMAS for two structures, measured with a Renishaw inVia Raman microscope (20 mw for less than 10 nmol and 2 mw for other concentrations, 3 s acquisition time, and 50× objective lens) at different CV concentrations: (c) mesh structure; (d) nanowire bundles.

well as its SERS activity requires electron and optical microscopic observations on the same region so as to ensure that the exact same particle is characterized (Fig. S6†). Therefore, in this work, a silicon wafer patterned by electron beam lithography was employed as a substrate to support the synthesized OMAS-10 (Fig. 5a). The Raman spectra for two kinds of OMAS-10 structures are shown in Fig. 5b, which are recorded at 514 nm excitation with the same CV concentrations, *e.g.* 10^{-7} M aqueous. The SERS spectra reveal the characteristic peaks of CV, for instance at 1172, 1371, and 1619 cm^{-1}, and correspond well to the ordinary Raman spectra of CV in the solid state and in aqueous solution. One can see that the intensities of the CV peak at ~1619 cm^{-1} are around 3200 and 6300 for mesh structures and nanowire bundles at 514 nm excitation wavelength, respectively (Fig. 5b). According to the procedure described in ref. 15 and 21–26 for the CV molecules, the EFs of the OMAS-10 are estimated to be about 4.85×10^8 for the mesh structure and 1.03×10^9 for the nanowire bundle. This result is consistent with that of theoretical calculation using the FDTD methods for two structures. To evaluate the limit of detection (LOD) for two kinds of structures of OMAS-10, a series of low concentrations of CV aqueous solution as SERS probe molecules ranging from 1 μM to 0.1 pM were measured. From Fig. 5c and d, the nanowire bundle structure of OMAS-10 demonstrates a better sensitivity with a LOD down to 0.1 pM even less. While for the mesh structure of OMAS-10, the Raman spectrum can be identified at the level of 0.1 nM for CV molecules. Thus, the OMAS-10, particularly for nanowire bundle structures, can be exploited as high-quality SERS based sensing detection.

Conclusion

In conclusion, we have successfully synthesized an ordered mesoporous Ag superstructure (OMAS-10) by the nanocasting process using mesoporous silica KIT-6 and SBA-15 as templates. The obtained structures with high density and uniform nanogaps (~1–3 nm) can be controlled by the parent template. Furthermore, such a silver superstructure as a SERS substrate exhibits a high sensitivity on the order of magnitude of $\sim 10^9$ and the detection limit of the OMAS-10 with nanowire bundles can reach 0.1 pM levels for CV molecules. The FDTD calculation reveals that the ordered silver superstructure has a uniform distribution of hot spots, which are particularly beneficial to the reproducibility for SERS. Therefore, we believe that the OMAS with a controlled nanoparticle size and uniform gap will be an effective SERS substrate for organic chemical molecules, biomolecules, even at the single molecule level.

Experimental section

Chemicals

KIT-6 was supplied by Tianjin University (Tianjin, China). SBA-15 was purchased from Nanjing XFNANO Material Tech. Co., Ltd. Silver nitrate ($AgNO_3$) was purchased from Sigma. Hexamethyldisilazane (HMDS) was purchased from Sinopharm Chemical Reagent Co., Ltd. Ethanol (C_2H_5OH) and sodium hydroxide (NaOH) were purchased from Tianjin Chemical corp.

Synthesis of OMAS-10 by the dip-calcination method

In order to improve long-range ordering in three dimensions according to the template direction, a modified dipping method was implemented. In this process, OMAS-10 was synthesized by following methods reported elsewhere.[27] Briefly, the silica surface of KIT-6 or SBA-15 was modified with methyl groups by refluxing a mixture containing 0.039 g of hexamethyldisilazane (HMDS), 30 mL of *n*-hexane and 0.2 g of calcined KIT-6 or SBA-15. The obtained material is denoted as HP-KIT-6 (hydrophobic KIT-6) or HP-SBA-15 (hydrophobic SBA-15). In order to synthesize the mesoporous silver, a solution containing 0.021 g of $AgNO_3$ (3 M) was impregnated into 0.035 g of the HP-KIT-6 or HP-SBA-15 through an incipient wetness method. After drying at 313 K for two days, the sample was heated to 573 K under nitrogen flow for 2 h. Then the silica template was completely removed by treating the composite material with a 3 M NaOH solution three times at 310 K. Finally, the product of the mesoporous silver was washed with acetone and distilled water several times and dried at room temperature.

Characterization

The morphology and structure of mesoporous templates and OMAS-10 were observed using a scanning electron microscope (SEM, JSM-7000F) and a transmission electron microscope (TEM, JEM 2100). The small-angle X-ray scattering (SAXS) data were obtained on a Bruker D8 Advance X-ray diffractometer with Cu Kα radiation (λ = 1.5406 Å). A scan rate of 0.018° min^{-1} was used to record the patterns in the 2θ range of 0.7°–3.0°. For measuring a large area of OMAS-10 at 10^{-7} M concentration of CV (as shown in Fig. 4a), the Raman spectra were measured with a confocal Raman microscope (LabRAM HR800) at the excitation wavelength of 514 nm from an argon ion laser, and the laser power was ~0.022 mW. The laser spot on a sample was ~0.8 μm in diameter in confocal mode. Raman signals were collected through the 100× objective in the backscattering geometry. The acquisition time was 2 s. For measuring the detection limit of OMAS-10, the Raman spectra were obtained by using a Renishaw inVia Raman microscope at room temperature through 50× objective of a Leica microscope (1 mm laser spots). The wavelength of the excitation laser used is 514 nm and the power is 20 mW at the sample of less than 10 nmol, and 2 mW for other concentrations. The exposure time was 3 s.

Acknowledgements

This work was supported by the National Natural Science Foundation of China (No. 11304188 and 51171139), the Doctoral Fund for New Teachers (No. 20130201110032 and 20110201120039), Fundamental Research Funds for the Central Universities (No. xkjc2014004) and the Scientific New Star Program in Shaanxi Province (No. 2012KJXX-03).

References

1 S. Nie and S. R. Emory, *Science*, 1997, **275**, 1102–1106.
2 K. Kneipp, Y. Wang, H. Kneipp, L. T. Perelman, I. Itzkan, R. R. Dasari and M. S. Feld, *Phys. Rev. Lett.*, 1997, **78**, 1667–1670.
3 D. K. Lim, K. S. Jeon, J. H. Hwang, H. Kim, S. Kwon, Y. D. Suh and J. M. Nam, *Nat. Nanotechnol.*, 2011, **6**, 452–460.
4 H. X. Xu, E. J. Bjerneld, M. Käll and L. Börjesson, *Phys. Rev. Lett.*, 1999, **83**, 4357–4360.
5 H. X. Xu, J. Aizpurua, M. Käll and P. Apell, *Phys. Rev. E*, 2000, **62**, 4318–4324.
6 W. Y. Li, P. H. C. Camargo, X. M. Lu and Y. N. Xia, *Nano Lett.*, 2009, **9**, 485–490.
7 Y. Fang, N. H. Seong and D. D. Dlott, *Science*, 2008, **321**, 388–392.
8 T. Thai, Y. Zheng, S. H. Ng and S. Mudie, *Angew. Chem., Int. Ed.*, 2012, **51**, 8732–8735.
9 A. Q. Chen, A. E. Deprince III, A. Demortiere, A. Joshi-Imre, E. V. Shevchenko, S. K. Gray, U. Welp and V. K. Vlasko-Vlasov, *Small*, 2011, **7**, 2365–2371.
10 H. Im, K. C. Bantz, N. C. Lindquist, C. L. Haynes and S. H. Oh, *Nano Lett.*, 2010, **10**, 2231–2236.
11 X. Liu, Y. Shao, Y. Tang and K. F. Yao, *Sci. Rep.*, 2014, **4**, 5835.
12 Y. P. Wu, Z. Fei, L. B. Yang and J. H. Liu, *Chem. Commun.*, 2013, **49**, 5025–5027.
13 Y. Kuroda and K. Kuroda, *Angew. Chem., Int. Ed.*, 2010, **49**, 6993–6997.
14 H. J. Wang, H. Y. Jeong, M. Imura, L. Wang, L. Radhakrishnan, N. Fujita, T. Castle, O. Terasaki and Y. Yamauchi, *J. Am. Chem. Soc.*, 2011, **133**, 14526–14529.
15 C. F. Tian, Y. H. Deng, D. Y. Zhao and J. X. Fang, *Adv. Opt. Mater.*, 2015, **3**, 404–411.
16 F. Kleitz, S. H. Choi and R. Ryoo, *Chem. Commun.*, 2003, 2136–2137.
17 M. H. Huang, A. Choudrey and P. D. Yang, *Chem. Commun.*, 2000, 1063–1064.
18 C. H. Ding, C. F. Tian, R. Krupke and J. X. Fang, *CrystEngComm*, 2012, **14**, 875–881.
19 W. E. Doering and S. M. Nie, *J. Phys. Chem. B*, 2002, **106**, 311–317.
20 A. Otto, The 'Chemical' (Electronic) Contribution to Surface-Enhanced Raman Scattering, *J. Raman Spectrosc.*, 2005, **36**, 497–509.
21 Y. Wang, M. Becker, L. Wang, J. Q. Liu, R. Scholz, J. Peng, U. Gösele, S. H. Christainsen, D. H. Kim and M. Steinhart, *Nano Lett.*, 2009, **9**, 2384–2389.
22 W. B. Cai, B. Ren, X. Q. Li, C. X. She, F. M. Liu, X. W. Cai and Z. Q. Tian, *Surf. Sci.*, 1998, **406**, 9–22.
23 J. X. Fang, S. Y. Du, S. Lebedkin, Z. Y. Li, R. Kruk, M. Kappes and H. Hahn, *Nano Lett.*, 2010, **10**, 5006–5013.

24 J. X. Fang, S. Y. Liu and Z. Y. Li, *Biomaterials*, 2011, **32**, 4877–4884.
25 C. F. Tian, C. H. Ding, S. Y. Liu, S. C. Yang, X. P. Song, B. J. Ding, Z. Y. Li and J. X. Fang, *ACS Nano*, 2011, **5**, 9442–9449.
26 Z. Liu, Z. Yang, B. Peng, C. Cao, C. Zhang, H. You, Q. Xiong, Z. Y. Li and J. X. Fang, *Adv. Mater.*, 2014, **26**, 2431–2439.
27 J. K. Shon, S. S. Kong, J. M. Kim, C. H. Ko, M. Jin, Y. Y. Lee, S. H. Hwang, J. A. Yoon and J. N. Kim, *Chem. Commun.*, 2009, 650–652.